ACS APPLIED MATERIALS & INTERFACES

RESEARCH ARTICLE

www.acsami.org

Ceramic Coatings of LA141 Alloy Formed by Plasma Electrolytic Oxidation for Corrosion Protection

Zhijun Li, Yi Yuan,* Pengpeng Sun, and Xiaoyan Jing

Key Laboratory of Superlight Materials & Surface Technology, Ministry of Education, Harbin Engineering University, Harbin 150001, P. R. China

ABSTRACT: Superlight Mg−Li alloy is a promising structural materials in aerospace, automobile, and electronics because of its excellent properties such as low density, high ductility, superior strength-to-weight ratio, and good damping ability. The fabrication of compact plasma electrolytic oxidation coatings with excellent corrosion resistance is valuable for the widespread application of Mg−Li alloy. Here we present a ceramic coating on the surface of Mg-14Li-1Al (LA141) alloy for corrosion protection via plasma electrolytic oxidation (PEO) in an alkaline silicate electrolyte with tungstate as an additive. X-ray photoelectron spectroscopy and thin film-X-ray diffraction analysis of coatings show that the surface coating is mainly comprised of Mg_2SiO_4, MgO and WO_3. Scanning electron microscopy observations have revealed that the dense and compact coating formed in the presence of tungstate has less structural imperfections in comparison to the control one fabricated without use of tungstate. The effect of oxidation time on the morphology and phase composition of coatings is also examined in detail.

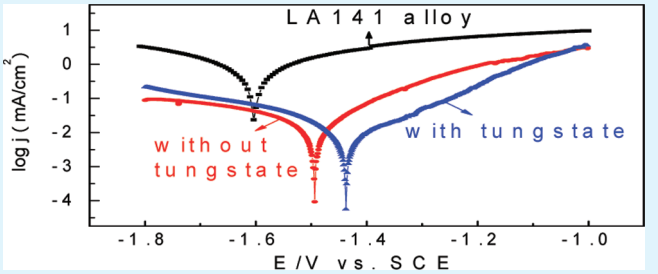

KEYWORDS: LA141 alloy, plasma electrolytic oxidation, tungstate

1. INTRODUCTION

As the lightest structural materials, Mg−Li alloys are widely utilized in the fields of aerospace, automotive, electronic and other industries.[1] All applications of Mg−Li alloys are based on the unique characteristics of higher strength-to-weight ratio, high specific stiffness, good machining property, good magnetic screening and shock resistance ability.[2−4] However, the poor corrosion resistance that results from the high chemical reactivity of magnesium and lithium has impaired the widespread practical application of Mg−Li alloys, especially in aggressive environments. Though many surface treatment techniques such as conversion treatment, electroless plating, anodizing, sol−gel, and physical vapor deposition[5−8] have been applied to improve corrosion resistance of the traditional magnesium alloys, researches carried out on corrosion resistance of Mg−Li alloy are limited.[9−14] Among these limited studies, most have focused on the conversion coatings; however, the brittle and thin conversion coatings are usually used for decoration and intermediate protection, and rarely used for long−term corrosion protection. So, it is necessary to develop surface modification technologies to improve corrosion resistance of Mg−Li alloys. Plasma electrolytic oxidation (PEO) as a relatively new electrochemical surface treatment technology based on anodic oxidation has been used to fabricate ceramic coatings in vivo on valve metals such as Al, Mg, and Ti.[15−19] The compact PEO coatings that adhere firmly to the substrate impart excellent properties, such as high hardness, wear resistance, anticorrosion and thermal stability.[20−23] The properties of the PEO coating are affected by many factors, of which a key determinant is the composition of electrolyte that can modify surface morphology, microstructure, and composition of the PEO coatings.[24−26]

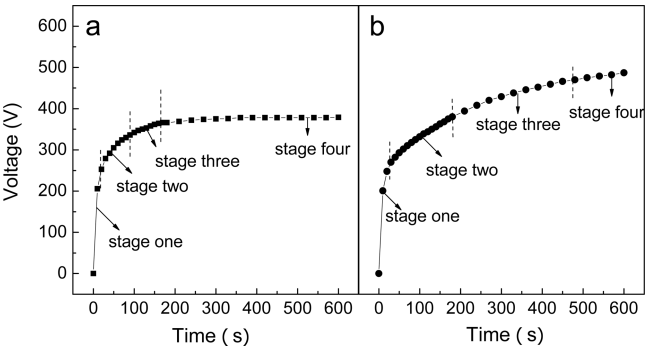

Figure 1. Voltage−time responses for PEO processes of LA141 alloy formed in an alkaline silicate electrolyte (a) without and (b) with the addition of tungstate.

The influence of electrolyte on the properties of oxide film formed on magnesium alloy via PEO technique has previously been studied.[20,27−30] However, fabrication and characterization of PEO coatings on Mg−Li alloys have not received an extensive attention. Our previous work has demonstrated that PEO coatings can be successfully fabricated on the surface of Mg−Li alloys.[31,32] But since the content of Li had not exceeded 5 wt %,

Received: July 1, 2011
Accepted: August 12, 2011
Published: August 24, 2011

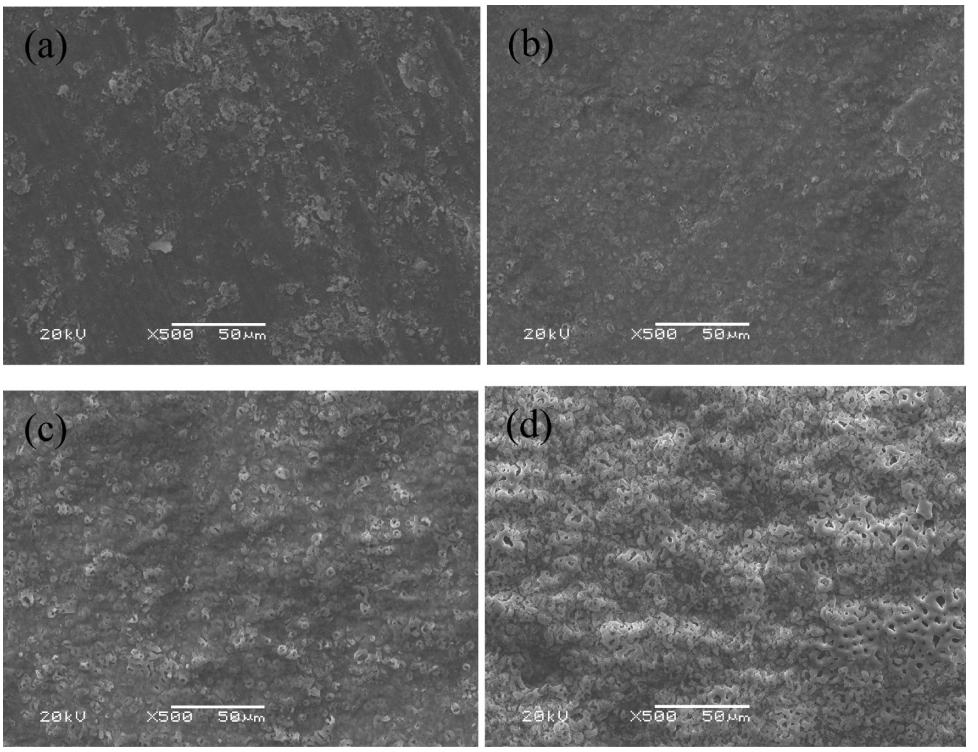

Figure 2. SEM images of PEO coatings formed at different PEO times formed in an alkaline silicate electrolyte with the addition of tungstate ((a) 30 s; (b) 90 s; (c) 180 s; (d) 600 s).

the alloys used in our previous research were merely composed of HCP α phase of Mg solid solution. According to the Mg−Li phase diagram, body-centered cubic (BCC) structured β phase of Li solid solution becomes the main composition of Mg−Li alloys when the content of Li is higher than 11.5 wt %. BCC structure shows better mechanical properties and worse corrosion resistance compared with HCP structure. In this paper, we fabricate a ceramic coating on BCC structured Mg−Li alloys (LA141) in a alkaline silicate/tungstate electrolyte via PEO technique with a clear motivation to investigate the evident influence of tungstate additive upon the surface morphology, microstructure, composition and corrosion resistance of the oxide coating via a joint analysis of SEM, TF-XRD, XPS, and potentiodynamic polarization. We also examine the PEO process conducted in alkaline silicate/tungstate electrolyte by taking a close look at the evolution of morphology and phase composition with oxidation time.

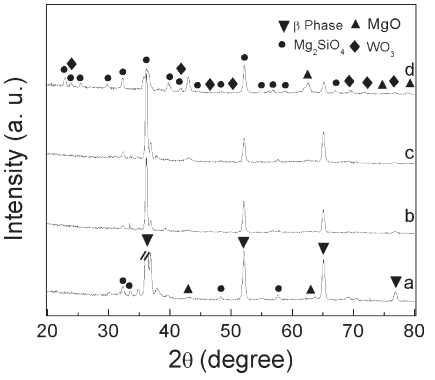

Figure 3. TF-XRD patterns of PEO coatings at different PEO times formed in an alkaline silicate electrolyte with the addition of tungstate ((a) 30 s; (b) 90 s; (c) 180 s; (d) 600 s).

2. EXPERIMENTAL SECTION

2.1. Preparation of PEO Coatings. The cylinder samples (height: 16 mm, diameter: 15 mm) of Mg−Li alloy (14 wt.% Li, 1 wt.% Al and Mg balance) were used as the substrate for the PEO coatings deposition. Prior to PEO treatment, the specimens were ground and polished with 800, 1000, 2000 grit silicon carbide paper to achieve a smooth surface, then ultrasonically cleaned in acetone and rinsed with ethanol, and finally dried in cool air. The alkaline silicate electrolyte was prepared from the solution of 15.0 g/L Na_2SiO_3 in distilled water with an addition of NaOH (2.0 g/L) and triethanolamine (5 mL/L) with and without the addition of Na_2WO_4 (0.6 g/L).

A pulsed DC electrical source was employed to control the voltage, current density and other electrical parameters such as frequency and duty cycle. The sample of Mg−Li alloy and a stainless steel container were used as anode and cathode, respectively. A cooling system was used to keep the temperature of the electrolyte at room temperature. The PEO process was conducted under constant current density. The appropriate electrical parameters were as following: frequency, 2000 Hz; duty cycle, 15%; current density, 5 A/dm^2. After PEO treatment of 10 min, the coated sample was taken out from electrolyte, rinsed thoroughly with distilled water and dried in cool air. Three samples were made under each condition to ensure the reliability of the experiments.

2.2. Coating Characterizations. The surface, cross-sectional morphologies and elemental compositions of PEO coatings were examined by JSM-6480A scanning electron microscopy (SEM) equipped with EDX (JEOL, Japan) and S4800 Field-emission scanning electron microscopy (Hitachi). The thickness of samples was measured with an eddy

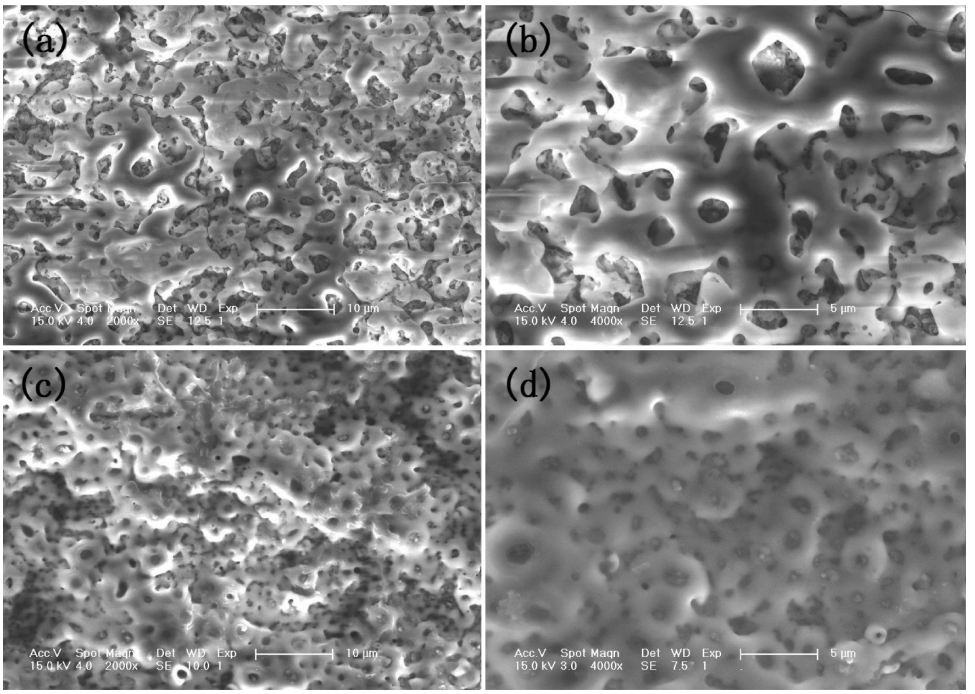

Figure 4. FE-SEM images of PEO coatings formed in an alkaline silicate electrolyte (a, b) without and (c, d) with the addition of tungstate.

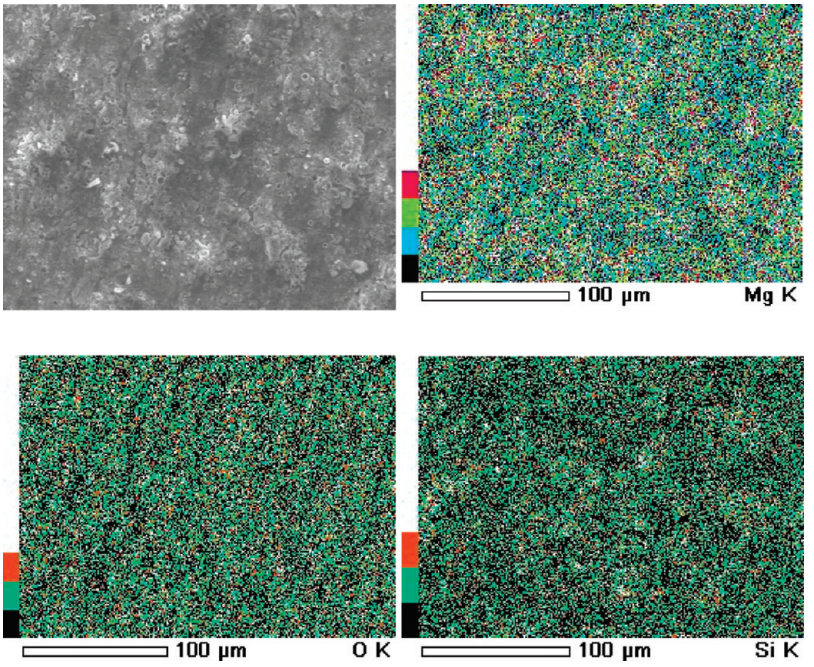

Figure 5. Element mappings in PEO coatings formed in an alkaline silicate electrolyte without the addition of tungstate.

current coating thickness measurement gauge (TT 230, Time Group Inc., China). The thickness data given were the average of ten measurements made at different locations. The phase composition of coatings was analyzed by thin-film X-ray diffraction (TF-XRD, Philip X'Pert, Holland), using a Cu K_α radiation as the excitation source at a grazing angle of 1°. The measurements were performed with a continuous scanning mode at a rate of 3° min^{-1}. The X-ray photoelectron spectroscopy (XPS) analyses were performed on a ESCALAB-MKII X-ray photoelectron spectrometer (VG Instruments, UK) using monochromatized Al K_α radiation (photon energy 1486.6 eV) as the excitation source and the binding energy of C1*s* (284.6 eV) as the reference. Xpspeak 4.1 software was used to analyze the data. Potentiodynamic polarization was performed on an eight channel VMP3/Z potentiostat (Princeton Applied Research) controlled by EC-lab software. All potentiodynamic polarization measurements were conducted in 3.5 wt % NaCl solution at room temperature using a conventional three-electrode cell with LA141 alloy or coated alloy as the working electrode, a saturated calomel electrode (SCE) as the reference electrode and a platinum plate as the

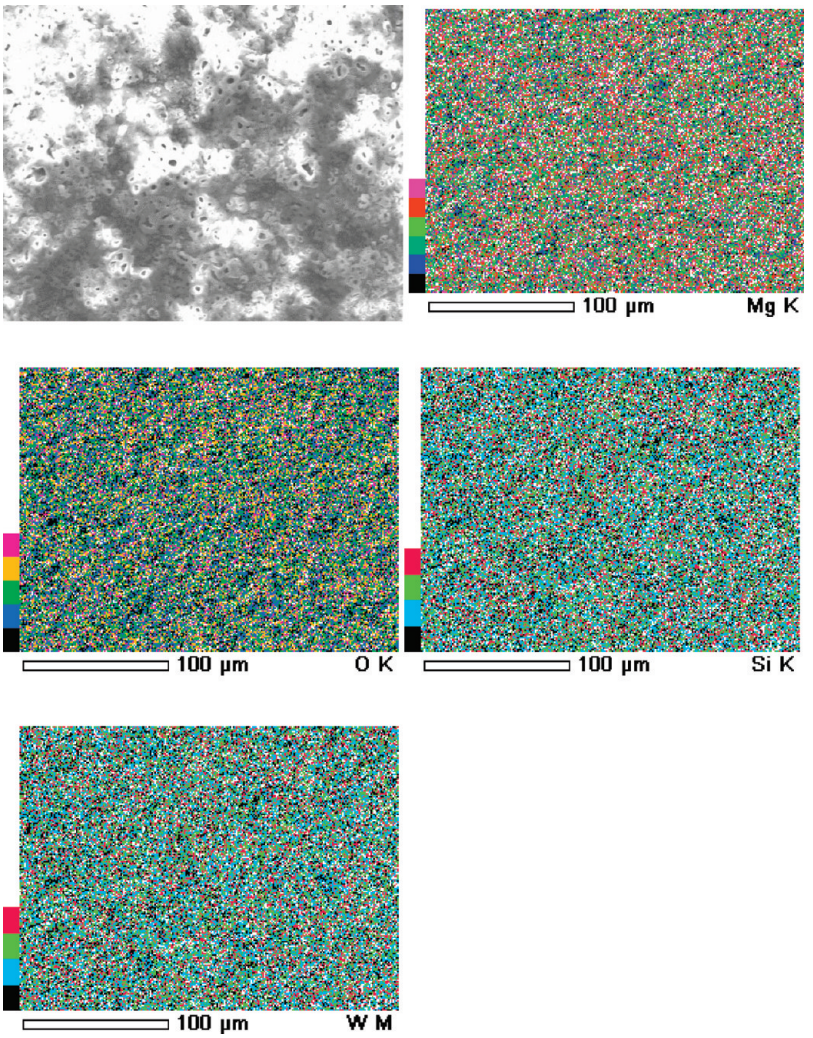

Figure 6. Element mappings in PEO coatings formed in an alkaline silicate electrolyte with the addition of tungstate.

counter electrode. For the potentiodynamic polarization test, scanning was from −1.8 to −1.0 V at a rate of 2.5 mV/s after an initial 5 min delay.

3. RESULTS AND DISCUSSION

3.1. Voltage−Time Curves for PEO Process. Figure 1 shows the voltage−time curves for the PEO process of LA141 alloy in an alkaline silicate electrolyte without (a) and with (b) the addition of tungstate.

The instantaneous variation of voltage was recorded every 10 s before the first 3 min and every 30 s after 3 min. The PEO processing of LA141 alloys is characterized by four different stages in each two curves. In the first stage, the voltage increases linearly with time, approximately. The alloy substrate dissolves at first and a thin barrier layer forms on the surface of LA141 alloy. In the second stage, a thin barrier layer breakdown and fine spark discharges appear. The voltage of the alloy treated in the alkaline silicate electrolyte is higher in the first two stages, and the rate of the voltage in the previous two stages is faster than the alloy treated in the alkaline silicate electrolyte with the addition of tungstate. In the third stage, the moving spark changes in shape, size, density and color. The increased rate of voltage for the alloy treated in the alkaline silicate electrolyte with the addition of tungstate is higher and the period of third stage is much longer than that of the alloy treated in the alkaline silicate electrolyte. We speculate that a thicker coating should be obtained by using tungstate as an additive. In the fourth stage, the large spark discharge is transferred to fine spark discharge and the number of spark discharges increases on the entire sample surface. The voltage increases from 366 to 379 V for LA141 alloy treated in alkaline silicate electrolyte. However, the voltage change is 8 V (from 479 to 487 V) for LA141 alloy treated in the alkaline silicate electrolyte with the addition of tungstate. After 9 min treatment, the whole sample surface is covered by golden sparks. The discharge sparks behavior of the PEO coating prepared in the alkaline silicate electrolyte without the addition of tungstate is different from our previous work.[31] The main reason is due to the different content of Li in the alloy substrate. When LA141 alloy is immersed in the electrolytes and acts as anode, Li compositions on the surface of alloys would be first oxidized and dissolved into the electrolytes. It is difficult to form uniform anodic oxidation coatings on the surface of the alloys due to the release of reactive Li compositions into the electrolytes. The addition of corrosion inhibitor tungstate is favorable for the formation of passive film on the surface of LA141 alloy, which is essential for the formation of oxide film under the applied voltage. Our

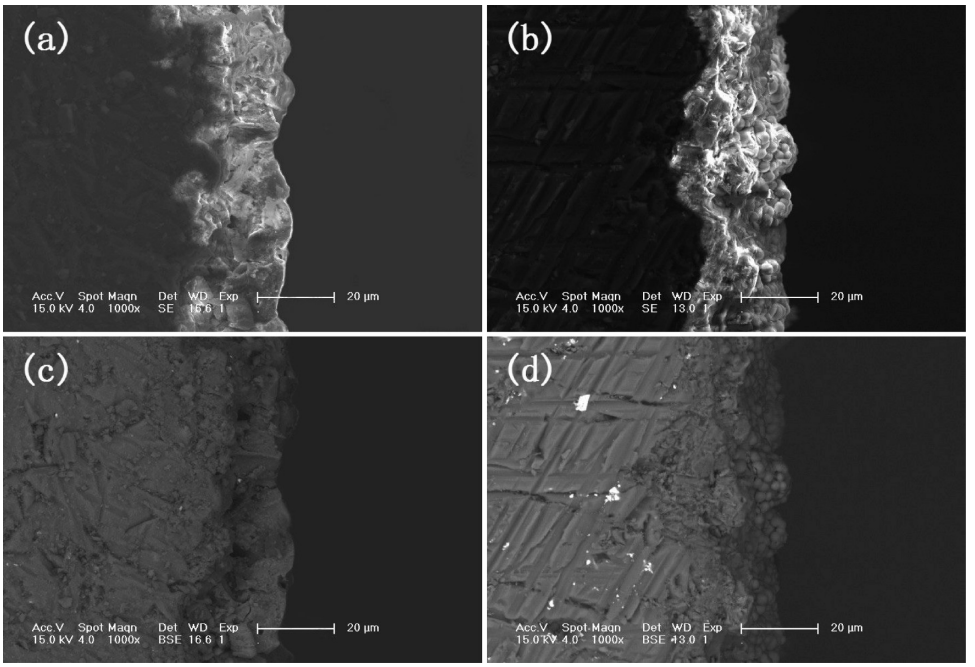

Figure 7. Cross-sectional FE-SEM images of PEO coatings formed in an alkaline silicate electrolyte (a) without and (b) with the addition of tungstate. The backscattered electron images of PEO coatings formed in an alkaline silicate electrolyte (c) without and (d) with the addition of tungstate.

experimental results indicate that the plasma discharge behavior of the alloy treated in the alkaline silicate electrolyte without the addition of tungstate is much fierce than that with the addition of tungstate. As proposed by Nie et al.,[33] strong discharges would make the coating more porous and elimination of strong discharges may facilitate the formation of inner layer with denser microstructure and less porosity. This implies that the addition of tungstate in the electrolytic solution may have impact on the PEO process and subsequently affect the formation and characteristics of the oxide coating.

3.2. Effect of Oxidation Time on PEO Coatings. *3.2.1. Morphology Characteristics of PEO Coatings Formed at Different PEO Times.* We investigate the structure of PEO coatings formed at different PEO times with scanning electron microscopy and TF-XRD. Figure 2 shows the SEM images of PEO coatings prepared in an alkaline silicate electrolyte with the addition of tungstate at different PEO times.

As shown in Figure 2a, only parts of the substrate is covered by porous PEO coating after PEO process of 30 s; traces of the polishing scratches before the PEO process are clearly observed. When PEO time attains 90 s (Figure 2b), nearly all the surface of the substrate is covered by a porous ceramic coating, and the grinding cracks have almost disappeared. As the oxidation time increase, the size and density of pores increase as well (Figure 2c). Figure 2d shows the SEM image of the coating obtained at 600 s. In compared with the PEO treatment of 180 s, the average size of the micropores increases and the number of micropores decreases, which is a typical morphology of PEO coating.

3.2.2. Phase Compositions of PEO Coatings Formed at Different PEO Times. TF-XRD patterns of PEO coatings formed in an alkaline silicate electrolyte with the addition of tungstate at different PEO times (30 s, 90 s, 180 s, and 600 s) are shown in Figure 3. When the PEO time is 30 s (Figure 3a), the diffraction peaks of β phase originating from the alloy substrate are still very strong, we can only observe weak diffraction peaks of Mg_2SiO_4

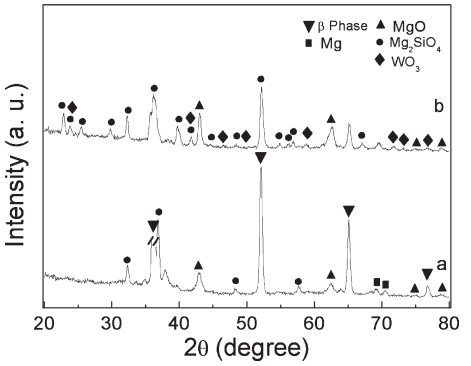

Figure 8. TF-XRD patterns of PEO coatings formed in an alkaline silicate electrolyte without (a) and with (b) the addition of tungstate.

and MgO in the TF-XRD pattern. The process of plasma electrolytic oxidation is actually the plasma discharge process, the temperature in the microdmain of discharge can reach 2000 °C, and the instantaneous pressure is about 100 MPa. First, Mg and Li element in the alloy substrate melt under high temperature and pressure produced by plasma discharge, then molten Mg and Li react rapidly with the oxygen atom on the surface of alloy and form MgO under the cold quenching of electrolyte. Subsequently, deposited MgO remelt and react with SiO_3^{2-} to produce Mg_2SiO_4. As the oxidation time increases, the intensity of peak of MgO increases and the intensity of β phase decreases. Because of the short oxidation time, the coatings produced after 90 and 180 s treatment are still thin, X-rays can easily penetrate the ceramic coatings to the substrate; therefore, the diffraction peaks of β phase come from the LA141 alloy substrate are still strong. After a PEO treatment of 600 s, as shown in Figure 3d, diffraction peaks of Mg_2SiO_4 and a new phase of WO_3 can be clearly detected.

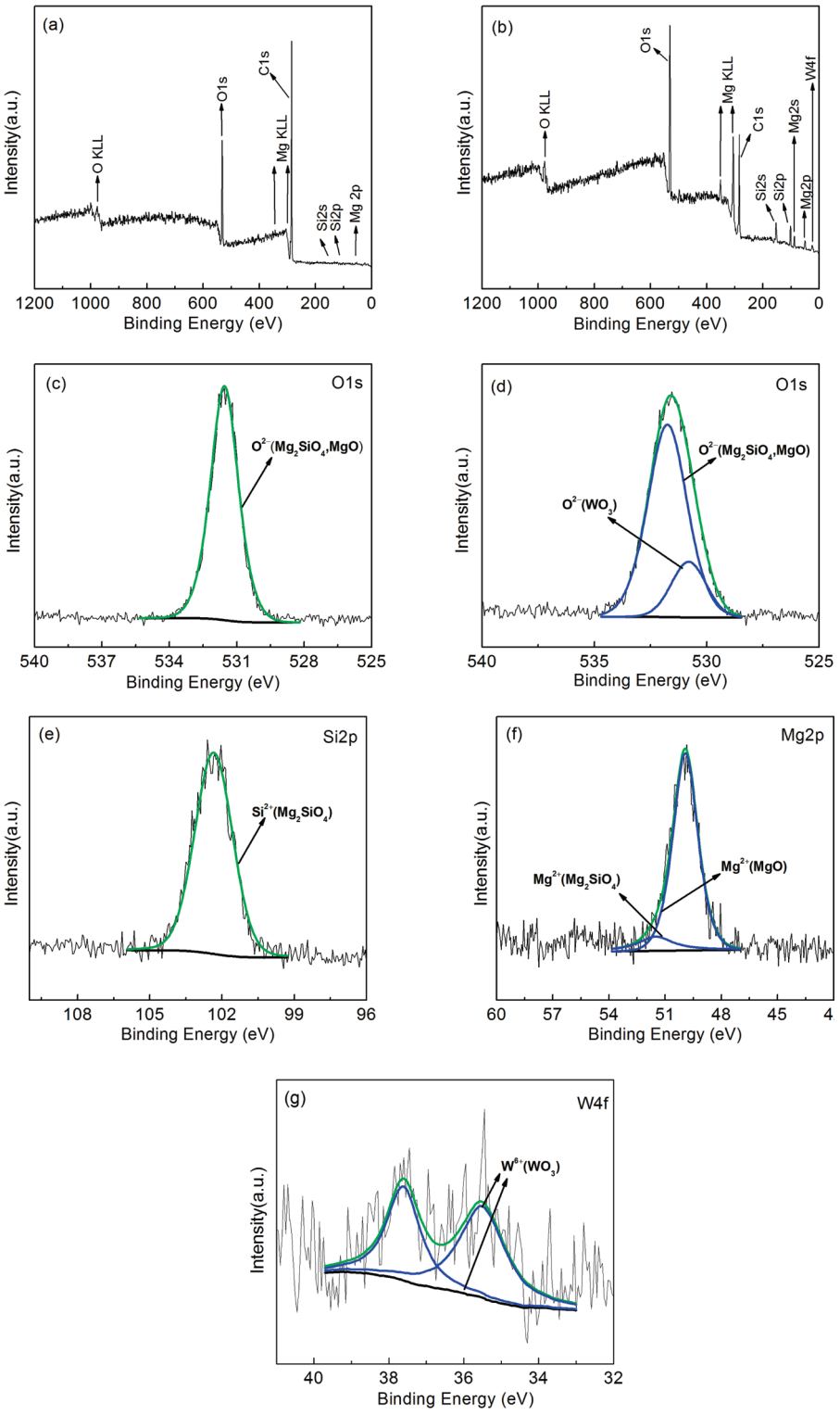

Figure 9. XPS spectra of PEO coatings formed in an alkaline silicate electrolyte without (a, the survey spectrum; c, the specific spectra of O 1s) and with the addition of tungstate (b, the survey spectrum; the specific spectra of d, O 1s, e, Si 2p, f, Mg 2p and g, W 4f). The black lines are XPS data. The green curve is the fitting of experimental data for coating, which can be decomposed into a superposition of two peaks shown as blue curves.

3.3. Morphology Characteristics of PEO Coatings. Figure 4 shows the surface morphologies of the PEO coatings formed in alkaline silicate electrolyte without tungstate (a, b) and with tungstate addition (c, d). We notice that a large number of pancake-like or lenticular-like micropores arrange disorderly on the rough PEO coating prepared in an alkaline silicate electrolyte without tungstate. Pores of different size range (0.7 to 4 μm) and shapes imply that different discharge types including strong, moderate and small contribute to the formation of oxide coating. The appearance of some microcracks is probably due to the

thermal stress generated under high temperature and high pressure. After introducing tungstate into the electrolyte as an additive, the morphology of PEO coating undergo dramatic change and a smoother and denser oxide coating with smaller micropores (1 to 2.5 μm) is formed. Besides, we cannot observe the existence of microcracks. Obviously, the evident morphology change can be related to different discharge behavior in the two kinds of electrolyte. Furthermore, we can tune the anticorrosion properties by adjusting the component of electrolyte. The results demonstrate that addition of tungstate into the electrolyte can favor the formation of a relatively uniform coating with less structure imperfections, which is consistent with the analysis of voltage−time curves.

The elemental mappings of PEO coatings formed in an alkaline silicate electrolyte without and with the addition of tungstate obtained by energy disperse X-ray analysis spectroscopy are presented in Figures 5 and 6, respectively.

It can be seen from Figure 5 that Mg, O, and Si signals from sample distribute uniformly on the surface of LA141 alloy. After introducing tungstate into the electrolyte, it can be seen that W signal from the sample is existent (Figure 6). It indicates that both substrate and species in the electrolyte take part in the reaction in the discharge channel and contribute to the formation of the coating.

Cross-sectional FE-SEM images of coatings formed in an alkaline silicate electrolyte without and with the addition of tungstate, formed in consequence of melting by plasma discharges and instantaneous quenching by the electrolyte, and integrated firmly due to sintering effect, onto the LA141 alloy substrate are shown in images a and b in Figure 7, respectively. It can be seen that the PEO coating is composed of an inner layer and an outer porous layer, the boundary between two layers is clear as shown in the backscattered electron images (Figure 7c,d). And there are micropores and microcracks in the cross-section images, but these micropores and microcracks are not connected each other or perforated through the entire oxide film, which reveals high bonding strength between them. The thickness of two coatings shown in the cross-sectional images is approximately 12 and 22 μm, respectively, which corroborate the data obtained from the thickness probe. After introducing tungstate into the electrolyte, the thickness of coating increases obviously, the micropore decreases in size and number, a denser oxide coating with less structure imperfections is obtained. The improvement of microstructure can efficiently enhance the corrosion resistance of PEO coating.

3.4. Phase Compositions of PEO Coatings. TF-XRD patterns of the PEO coatings are shown in Figure 8. It is clearly shown that the PEO coating prepared in an alkaline silicate electrolyte is mainly composed of Mg_2SiO_4 and MgO, and strong diffraction peaks of β phase from the substrate are evident. This can be explained by the penetration of X-ray into substrate due to a thin coating (12 μm) as shown in Figure 7a. Although the diffraction peaks of WO_3 are detected in TF-XRD pattern of PEO coating formed in an alkaline silicate electrolyte with the addition of tungstate. As the intensity of β phase decreases, diffraction peaks of MgO and Mg_2SiO_4 are detected due to the formation of PEO coating. The formation of the WO_3 results from the reaction of WO_4^{2-} ions in the discharge channels, as suggested by Zheng et al.[34]

$$2WO_4^{2-} - 4e \rightarrow 2WO_3 + O_2\uparrow$$

3.5. Chemical Compositions of PEO Coating. The XPS survey spectrum (Figure 9a) shows that the PEO coating formed in the alkaline electrolyte without the addition of tungstate is mainly composed of Mg, Si and O. The XPS survey spectrum (Figure 9b) indicates that the PEO coating formed in the alkaline electrolyte with the addition of tungstate is mainly composed of Mg, Si, O, and W. The O 1*s* XPS spectra of two coatings show dramatic differences (Figure 9c,d), the single O 1*s* peak at 531.75 eV, typical for Mg_2SiO_4 and MgO, can be resolved into two peaks at about 531.75 and 530.80 eV. The O 1*s* peak around 531.75 eV corresponds to Mg_2SiO_4 and MgO, and 530.80 eV corresponds to WO_3. The photoelectron peaks of Si 2p, Mg 2p, and W 4f are shown in Figures 9e−g, respectively. The Si 2p peak at 102.34 eV associates with Mg_2SiO_4. The XPS spectra of Mg 2p around 49.92 and 51.50 eV correspond to MgO and Mg_2SiO_4, respectively. The binding energy peaks located at 35.50 and 37.61 eV are attributed to spin−orbit splitting of the W 4*f* components (W $4f_{7/2}$ and W $4f_{5/2}$), which are in good agreement with those of tungsten(VI) trioxide power.[35] The XPS results are consistent with the TF-XRD results above.

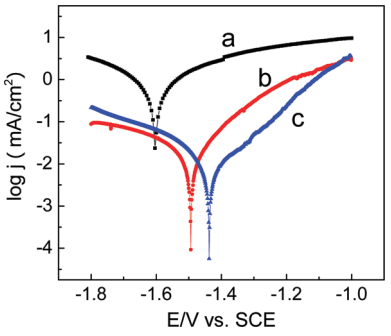

Figure 10. Potentiodynamic polarization curves of LA141 alloy substrate (a), PEO coatings formed in an alkaline silicate electrolyte without (b) and with (c) the addition of tungstate.

Table 1. Electrochemical Parameters Related to Potentiodynamic Polarization Curves

sample	E_{corr} (V)	i_{corr} (A/cm^2)	R_p (Ω)
LA141 alloy	−1.604	7.1×10^{-4}	92
without tungstate	−1.490	2.0×10^{-5}	2381
with tungstate	−1.402	8.8×10^{-6}	4243

3.6. Anti-Corrosion Analysis of the PEO Coatings. Anticorrosion behavior of LA141 alloy and PEO coatings formed in an alkaline silicate electrolyte without and with the addition of tungstate are evaluated by potentiodynamic polarization in 3.5 wt % NaCl solution. In a typical polarization curve, lower corrosion current density, positive corrosion potential and higher polarization resistance correspond to lower corrosion rate and better corrosion resistance of the coating. The obtained potentiodynamic polarization curves and related parameters including the corrosion potentials (E_{corr}), corrosion current densities (i_{corr}) and polarization resistance (R_p) are shown in Figure 10 and Table 1, respectively.

From Figure 10 and Table 1, the corrosion potential of the PEO coating prepared in an alkaline silicate electrolyte shifts about 114 mV in a positive direction, the corrosion current density decreases approximately 1 order of magnitude and the polarization resistance increases about 1 order of magnitude compare with the LA141 alloy substrate. However, after the PEO treatment in an alkaline silicate electrolyte with the addition of

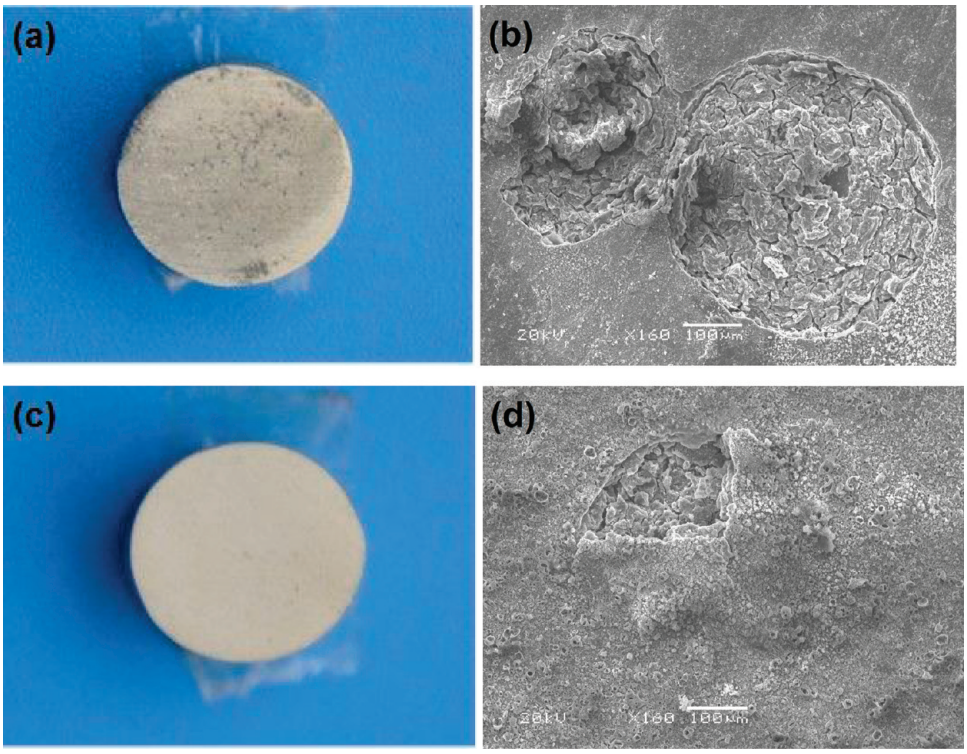

Figure 11. Photos and SEM images of PEO coatings formed in an alkaline silicate electrolyte without (a, b) and with (c, d) the addition of tungstate after potentiodynamic polarization test.

tungstate, the corrosion potential of the PEO coating shifts 202 mV in a positive direction. The corrosion current density decreases about 1 order of magnitude and the polarization resistance increases from 2381 Ω to 4243 Ω compared to the PEO coating formed in an alkaline silicate electrolyte. The experimental results clearly elucidate that the anticorrosion properties of the LA141 alloy substrate are improved greatly by the PEO coating formed in an alkaline silicate electrolyte with the addition of tungstate.

3.6. Surface Morphology Characteristics of PEO Coatings after Potentiodynamic Polarization Test. As depicted in Figure 11a, after a potentiodynamic polarization test there is some evident corrosion damages of the PEO coating formed without the addition of tungstate. A higher magnification micrograph (Figure 11b) also demonstrates severe localized corrosion damages of this film. Two corrosion pits with diameter of 484 and 288 μm are observed and many microcracks distribute on the corrosion pits. However, the addition of tungstate into the alkaline silicate electrolyte results in a PEO coating without significant corrosion damage as displayed in Figure 11c. Only a small sector is observed on the SEM image of the PEO coating formed with the addition of tungstate after a potentiodynamic polarization test (Figure 11d). The difference in corrosion morphologies could be ascribed to different properties and structure of the PEO coatings. The main corrosion type of the two kinds of PEO coatings in chloride containing solution is pitting corrosion. The pitting corrosion is induced when the corrosive intermediate (Cl^-) transfers through the porous PEO coating and arrives at the substrate. The corrosion pits on the PEO coatings are due to the corrosion products moving away from the coating and substrate into the NaCl solution.

4. CONCLUSIONS

We have obtained an anticorrosion and uniform ceramic coating mainly composed of MgO, Mg_2SiO_4 and WO_3 on the superlight LA141 alloy via PEO technique in an alkaline silicate/tungstate electrolyte. The corrosion resistance of PEO coating has been improved significantly using tungstate as additive in the electrolyte, which is probably due to the formation of thermodynamically stable Mg_2SiO_4 and WO_3 phase and substantial morphology and microstructure change of coating. The corrosion type of the PEO coating in a chloride containing solution is pitting corrosion. This method offers distinct advantages over other techniques in that it is reproducible, compatible with a variety of substrate types, and potentially scalable for industrial applications.

AUTHOR INFORMATION

Corresponding Author

*Tel: +86 451 82569890. Fax: +86 451 82569890. E-mail: yi.yuan@hrbeu.edu.cn.

ACKNOWLEDGMENT

National "863" Project (2006AA03Z510), Harbin Engineering University Basic Research Foundation (HEUFT 07055), and the Foundation for Youth Science and Technology innovation Talents of Harbin of China (2008RFQXG036) have supported this work.

REFERENCES

(1) Song, J. M.; Wen, T. X.; Wang, J. Y. *Scr. Mater.* **2007**, *56*, 529–532.

(2) Yang, L. H.; Li, J. Q.; Zheng, Y. Z.; Jiang, W. W.; Zhang, M. L. *J. Alloys Compd.* **2009**, *467*, 562–566.
(3) Crawford, P.; Barrosa, R.; Mendez, J. *J. Mater. Process. Technol.* **1996**, *56*, 108–118.
(4) Yamauchi, N.; Ued, N.; Okamoto, A.; Sone, T.; Tsujikawa, M.; Oki, S. *Surf. Coat. Technol.* **2007**, *201*, 4913–4918.
(5) Yong, Z. Y.; Zhu, J.; Qiu, C.; Liu, Y. L. *Appl. Surf. Sci.* **2008**, *255*, 1672–1680.
(6) Araghi, A.; Paydar, M. H. *Mater. Des.* **2010**, *31*, 3095–3099.
(7) Chen, X. M.; Li, G. Y.; Lian, J. S. *Appl. Surf. Sci.* **2008**, *255*, 2322–2328.
(8) Guo, X. H.; An, M. Z.; Yang, P. X.; Li, H. X.; Su, C. N. *J. Alloys Compd.* **2009**, *489*, 482–497.
(9) Sharma, A. K. *Met. Finish* **1989**, *87*, 173–174.
(10) Sharma, A. K.; Rani, R. U.; Bhojaraj, H. *J. Appl. Electrochem.* **1993**, *23*, 500–507.
(11) Shao, Y. W.; Huang, H. M.; Zhang, T.; Meng, G. Z.; Wang, F. H. *Corros. Sci.* **2009**, *51*, 2906–2519.
(12) Yang, L. H.; Li, J. Q.; Yu, X.; Zhang, M. L.; Huang, X. M. *Appl. Surf. Sci.* **2008**, *255*, 2338–2341.
(13) Yang, L. H.; Zhang, M. L.; Li, J. Q. *J. Alloys Compd.* **2009**, *471*, 197–200.
(14) Gao, L. L.; Zhang, C. H.; Zhang, M. L.; Huang, X. M. *J. Alloys Compd.* **2009**, *485*, 789–793.
(15) Malyshev, V. N.; Zorin, K. M. *Appl. Surf. Sci.* **2007**, *254*, 1511–1516.
(16) Xue, W. B.; Wang, C.; Chen, R. Y.; Deng, Z. W. *Mater. Lett.* **2002**, *52*, 435–441.
(17) Duan, H. P.; Du, K. Q.; Yan, C. W.; Wang, F. H. *Electrochim. Acta* **2006**, *51*, 2898–2908.
(18) Bayati, M. R.; Moshfegh, A. Z.; Golestani−Fard, F. *Electrochim. Acta* **2010**, *55*, 2760–2766.
(19) Song, H. J.; Shin, K. H.; Kook, M. S.; Oh, H. K.; Park, Y. J. *Surf. Coat. Technol.* **2010**, *204*, 2273–2278.
(20) Ghasemi, A.; Raja, V. S.; Blawert, C.; Dietzel, W.; Kainer, K. U. *Surf. Coat. Technol.* **2008**, *202*, 3513–3518.
(21) Sabatini, G.; Ceschini, L.; Martini, C. *Mater. Des.* **2010**, *31*, 816–828.
(22) Nie, X.; Leyland, A.; Song, H. W.; Yerohkin, A. L.; Dowey, S. J. A. Mattews *Surf. Coat. Technol.* **1999**, *116−119*, 1055–1060.
(23) Yerokhin, A. L.; Lyubimov, V. V.; Ashitkov, R. V. *Ceram. Int.* **1998**, *24*, 1–6.
(24) Liang, J.; Srinivasan, P. B.; Blawert, C.; Dietzel, W. *Electrochim. Acta* **2009**, *54*, 3842–3850.
(25) Cakmak, E.; Tekin, K. C.; Malayoglu, U.; Shrestha, S. *Surf. Coat. Technol.* **2010**, *204*, 1305–1313.
(26) Bala Srinivasan, P.; Liang, J.; Blawert, C.; Stormer, M.; Dietzel, W. *Appl. Surf. Sci.* **2010**, *256*, 4017–4022.
(27) Liang, J.; Guo, B. G.; Tian, J. *Appl. Surf. Sci.* **2005**, *252*, 345–351.
(28) Xue, W. B.; Deng, Z. W.; Chen, R. Y.; Zhang, T. H. *Thin Solid Films* **2002**, *372*, 114–117.
(29) Wang, J.; Li, D. D.; Liu, Q.; Yin, X. *Electrochim. Acta* **2010**, *55*, 6897–6906.
(30) Song, L.; Kou, Y.; Song, Y.; Shan, D.; Zhu, G.; Han, E. H. *Mater. Corros.* **2011**, *62*, 1–9.
(31) Liu, J. Y.; Lu, Y.; Jing, X. Y.; Yuan, Y.; Zhang, M. L. *Mater. Corros.* **2009**, *60*, 865–870.
(32) Sun, P. P.; Lu, Y.; Yuan, Y.; Jing, X. Y.; Zhang, M. L. *Surf. Coat. Technol.* **2011**, *205*, 4500–4506.
(33) Hussein, R. O.; Nie, X.; Northwood, D. O. *Surf. Coat. Technol.* **2010**, *205*, 1659–1667.
(34) Zheng, H. Y.; Wang, Y. K.; Li, B. S.; Han, G. R. *Mater. Lett .* **2005**, *59*, 139–142.
(35) Cheng, L. F.; Zhang, X. T.; Liu, B.; Wang, H. Z.; Li, Y. C.; Huang, Y. B.; Du, Z. L. *Nanotechnology* **2005**, *16*, 1341–1345.